Wave formation on a shallow layer of flowing grains

By SHYAM N. PRASAD[1], DIPANKAR PAL[1]
AND MATHIAS J. M. RÖMKENS[2]

[1]University of Mississippi, University, MS 38677, USA
[2]National Sedimentation Laboratory, Oxford, MS 38655, USA

The phenomenon of longitudinal waves in shallow grain flows has been studied through laboratory experiments. The transport process of spherical particles on a metallic chute has been characterized for this purpose. The wave mode of material transport could be measured within selected combinations of flow parameters such as the angular inclination of the chute, the mean size of the grains and the mass flow rate. It has been observed that the moving particles tend to redistribute systematically in the direction of mean flow. As a result, nonlinear longitudinal waves evolve on the surface of the chute. Observations of the predominantly rolling mode of particle motion revealed significant particle dispersion away from the wavefronts. The frequency of inter-particle collisions was low in the dispersed flow regions but increased rapidly near the wavefronts to dissipate the excess kinetic energy, thus resulting in a large increase in the average volumetric solid fraction. In order to explain the appearance of discontinuities in the volumetric solid fraction, a theoretical model that preserves the overall balance of energy and allows a discontinuous periodic solution is examined here. The depth-averaged dispersed flow of the grains has been approximated by equations of motion similar to those of shallow fluid flow. The resistance to the rolling motion of the particles is expressed in terms of the hydrodynamic drag force. The theoretical model predicts the flow criterion for which the longitudinal waves would be self-sustaining.

1. Introduction

The present study was motivated by a need to understand the mechanics of sediment transport in upland areas of a watershed where the water flow depths are small and the associated Froude number (*Fr*) is high. The sediment consists primarily of soil detached by rainfall and covers the size range from clay particles to particle aggregates of up to a few millimetres in diameter. These overland shallow flows at high slopes are characterized by the presence of periodic waves called 'roll waves' in the hydraulic literature. Our observations in preliminary laboratory experiments with sediment-laden overland flow situations indicated that the unsteady mode of sediment transport primarily imitates the water waves. For a given limited set of hydraulic conditions of water flow at shallow depth (usually less than 1 cm), the momentum transport of sediments occurred in the form of a progression of intermittent slugs (or waves). These sediment waves seemed to follow the water waves at a certain phase difference, but the time-averaged measurements of the overall transport rates were fairly steady. The time-averaged amount of transported sediment

depended on its availability and reached a maximum for certain combinations of water discharge rate and channel slope. Ng & Mei (1994) have investigated the Newtonian and non-Newtonian behaviour of shallow flows of power-law fluids where permanent roll waves evolve as a result of nonlinear steepening of the free surface. Their linear stability analysis, however, does not predict a preferred wavelength for the waves generated out of infinitesimal disturbances. In his review paper, Iverson (1997) discussed the physics of surface wave motion in debris flows which carry a substantial amount of viscous pore fluid in the mixture of poorly sorted grains. In his experiments, the interstitial pore fluid contributed largely to the dynamics of wave tails whereas the structure of the wavefronts of solid materials was dominated only by particle collisions. The dynamic interactions between the two phases in our shallow channel flow experiment is quite intriguing as well, but difficult to comprehend through macro-scale experiments due to additional fluid turbulence effects. Since the solid phase shows organization within itself, laboratory experiments involving the flow of dry granular material under gravity may help in understanding the transport mode of a thin sheet of particulates. This prompted us to pursue the present research involving shallow flows of dry granular materials.

In the rapid dispersed flow regimes that appear in our experiments at shallow depths, each micro-scale solid particle moves independently of its immediate neighbours instead of moving as a bulk. The particles exhibit a rolling motion instead of sliding on the inclined surface except when they undergo saltation as they leave the bed due to non-uniformity in either their own geometry or that of the bed. If the depth of flow (h) remains very small (typically of the order of a millimetre for 88–250 μm diameter particles), the ratio of local flow depth to the average particle diameter (d_{av}) is also significantly small (typically, $h/d_{av} < 5$ from visual observation of the rarefied domains). In the shallow flow region, the particle dispersion in the two-phase medium occurs primarily in the direction of flow. This is due to the anisotropy in the momentum transfer process between loosely oriented particles. As a result of this longitudinal dispersion in the medium, the depth-averaged solid fraction of the mixture varies primarily in the direction of mean flow. The dispersion is prevalent in the acceleration domain of the evolving wavelengths and the particle velocity reduces rapidly near the wavefronts. When this sudden deceleration becomes significant, discontinuities appear in the volumetric solid fraction. The inter-particle distance changes by orders of magnitude (i.e. from dilute to concentrated) as the waves pass through the medium. In contrast to longitudinal waves in shallow granular flows, the phenomenon of lateral instabilities in granular media has recently been reported in an inclined bed experiment (Pouliquen, Delour & Savage 1997) and in a rotating cylinder experiment (Fried, Shen & Thoroddsen 1998). In these cases, the physical segregation of particles in different size ranges has resulted in lateral instabilities of different kinds as the overall flow kinetic energy was varied. The exact mechanism of such instabilities is not yet clearly understood. Though apparently similar instabilities are also encountered in certain cases of our experiment, the mechanism of longitudinal waves appears to be quite distinct and more dominant in the overall process. Therefore, only the longitudinal wave mode of transport is explored at present.

The process of energy transfer in shallow flows of granular materials under gravity is quite distinct from dense granular flows. Here, the flow energy is supplied by the gravitational force so that the kinetic energy of the particles continues to grow. In our experiments, a significant amount of energy dissipation occurred through resistive forces on the rolling motion of individual particles. The loss of energy is caused primarily through viscous drag on the particles by the interstitial fluid (i.e. air);

friction from the bed and sidewalls plays a rather minor role. The energy lost in inter-particle collisions also seems to be insignificant in the dispersed regions where the frequency of collisions remains small. However, the collisional frequency increases sharply at the wavefront and results into a significant loss of kinetic energy in the form of a shock. We initially expected that the Coulombic type of friction between the particles and the channel bed would control the dynamics of the flow. However, a careful qualitative observation of the moving particles revealed that the predominant motion is in the rolling mode with intermittent saltations from the channel bed. Therefore, it can be expected that the time- and space-averaged extent of resistance due to Coulomb friction should have a minimal effect on the overall transport process. Theoretical calculations of the wave velocities (details in §5) compared quite closely with the experimental measurements when the Reynolds-number-dependent drag force on the rolling particles was considered to be the primary source of energy dissipation. The response, based on the solutions of the nonlinear wave model, predicted overdamping due to sliding Coulombic friction and underpredicted the corresponding wave velocities by at least a factor of 4 in the present range of material flow rates.

The continued acceleration of the rolling particles on the inclined plane gives rise to random components of velocities, thereby increasing the possibility of energy loss through dissipation of granular temperature. The particle concentrations and, hence, the frequency of inter-particle collisions increases rapidly near the discontinuities of the evolving flow structures. It appears that there is a queuing effect which results into an energy-cyclic process that consists of a high kinetic energy domain in the region of accelerated flow and the shock domain where increased random components of particle velocity dissipate energy. Because of the success of the St. Venant equations of open channel flow in predicting nonlinear wave motions due to a similar energy redistribution process, we closely follow the same mathematical principles (Dressler 1949) to derive similar conservation equations for shallow granular flows. Though all the assumptions of a continuum do not hold strongly in such a dispersed medium, the justification in extending the continuum approach to rarefied grain flows lied in the cyclic characteristics of kinetic energy generation and dissipation processes in the two-phase medium. The resulting equations were amenable to analytical solutions of discontinuous periodic response by joining together sections of a continuous solution through the regions where inter-particle collisions dissipate energy. Thus, the present chute-flow experiments, in conjunction with the proposed mathematical model, attempt to explain the mechanism of progressive longitudinal waves in shallow grain flows.

2. Experimental procedure and flow conditions

The present experimental study was conducted at the National Sedimentation Laboratory in Oxford, Mississippi as a part of an ongoing research project on upland erosion control. The chute flow experiments were carried out in an inclined open channel as shown in figure 1. The width and length of the channel were 57 mm and 3.6 m, respectively. The width of the channel was large compared to average particle diameters (88–250 μm). Though the presence of sidewalls causes lateral shearing of the shallow flow, it does not alter the mechanism of evolving longitudinal waves. The particles were observed to undergo free rolling motion with intermediate saltations under impact with other particles and the bed. Therefore, any estimate of the number of particle layers (N) in these dispersed flow regions had a high degree of uncertainty.
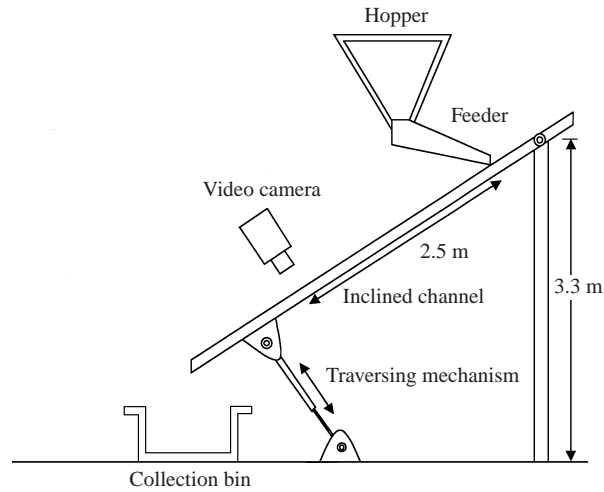
FIGURE 1. Experimental arrangement of inclined channel for studying shallow granular flows.

Only qualitative observation and experimenter's judgement are used to suggest that the space-averaged number of particle layers varied from less than one to about four in the low-density regions of the periodic structures. On the other hand, the number increased rapidly (say, twenty or more) in the 'shock region' and provided an avenue for escape of excess energy through generation of substantial fluctuation energy, commonly known as 'granular temperature'. The angle of inclination of the chute (θ) was varied in the range of 25° to 40° with the help of a traversing mechanism at the downstream end of the channel. Experimental data were obtained at three different angular inclinations: $\theta = 30°$, 35° and 38°. The maximum flow depth at the wavefronts was about 3 mm at the highest flow rates (Q) of the particles. Since the flow depth was much smaller at lower feed rates, the measurement of gradually varying depth of flow with a depth gauge had even larger uncertainties. Johnson, Nott & Jackson (1990), in a similar chute flow experiment, have revealed the inadequacy of current experimental techniques in providing accurate estimate of flow depth in dispersed granular flows. In particular, the dispersed and shallow flows of spherical grains produce large-amplitude saltations which tend to lead to overestimation in the traditional measurements of flow depth in gas–solid flows. Therefore, flow depth measurements are not reported here. The volumetric solid fraction of the flowing material could not be measured with satisfactory accuracy using any of the conventional techniques (like periodic sampling). Also, the intrinsic longitudinal variation of solid fraction within one wavelength of flow cannot be estimated from time-averaged measurements.

Solid glass spheres were used in this experimental study as the particulate medium. The specific gravity of the material was 2.5. The three different ranges of particle size were 88–125 μm, 125–177 μm and 177–250 μm, respectively. In each size range, 85% of the particles were true spheres. On the upstream end of the inclined channel, a hopper–feeder arrangement was installed to introduce the spherical glass beads onto the channel bed. The conical hopper and the channel-shaped feeder were equipped with individually controllable magnetic vibrators. The flow rate of the solid particles could be uniformly varied by changing the hopper opening and the excitation frequency of these vibrators. The hopper–feeder system was physically isolated from the inclined channel so that no vibration could directly propagate to the stationary

channel. The frequency of vibration of the hopper–feeder arrangement had no effect on the time scales of the evolving periodic flow structures since the two frequencies were different by at least an order of magnitude. The discharge rate of material out of the hopper–feeder arrangement was periodically sampled over short periods of time (between 15 and 30 s) to ascertain that there was no intrinsic periodicity in the material input rate to the inclined channel. Since the entry conditions in a chute flow experiment can control the initial rheological behaviour of the particulate medium (Johnson *et al.* 1990), the fall height of the solid spheres from the outlet of the feeder to the channel bed was kept constant at 40 mm. This created a condition of dilute entry of grains and avoided any material pile-up in the entry section of the experimental channel. The fall height was minimized to reduce the growth of flow transients in the initial section of the inclined channel. For the entire range of flow rates, the solid particles were observed to form the initial wave patterns within the first 0.5 m from the feeding point.

In order to measure the large-scale features of the granular flows, a video camera was positioned at a distance of 2.5 m from the feeding point on the channel. The time resolution of the camera was $\frac{1}{60}$th of a second. For the purpose of measuring the wave velocity (c) and wavelengths (λ) of the periodic structures on the channel bed, the flow of the granular solids was videotaped each time for a period of 1 min. The average mass flow rate (Q) of the granular solids was determined by intercepting the particles in a collection bin during the 1 min interval. The flow rate did not vary by more than 2% during this period. In our experiments, the overall range of mass flow rate was between 100 and 2800 g min^{-1} at different angular inclinations of the chute and the measurement uncertainty in Q was within $\pm7\%$. The measured wave velocities were within the range of 0.3 to 2.6 m s^{-1}. The wave velocity was measured for the most dominant longitudinal wavelength for a given set of Q and d_{av}. The uncertainty in wave velocity measurements was less than $\pm10\%$ for all the measurements. The average wavelength was obtained by averaging all the observed wavelengths at the measurement station during the 1 min period. Due to intrinsic nonlinearities and dispersion, the shallow granular transport at times appears to possess waves in the form of forerunners moving with higher speed than the observed periodic waves. Also, under some flow conditions, multiple lateral wavefronts were observed and the wavelength estimations, therefore, had higher uncertainties (maximum standard deviation of approximately $\pm26\%$).

3. Experimental results

The results of the experimental study of shallow chute flows of granular solids show that the wave patterns evolved on the channel bed once the two-phase medium overcame the initial transient motions of the solid particles. As the spherical particles came out of the feeder and dropped on the stationary channel bed, their dominant periodic motion in the longitudinal direction ensued after several cycles of saltation at large amplitudes. These transient motions of the particles died down in less than 0.5 m from the feeding point on the channel. For all the experimental and theoretical data reported hereafter, each size range of the granular material has been represented by its average diameter. The average particle diameter (d_{av}) has been assumed to be the arithmetic mean of its limiting sizes (i.e. $d_{av} = (d_{min} + d_{max})/2$, where d_{min} and d_{max} are the minimum and maximum particle diameters in a size range). The average particle diameter obtained this way is a true representation of the size range since the size concentrations in these commercially manufactured mixtures of glass beads showed
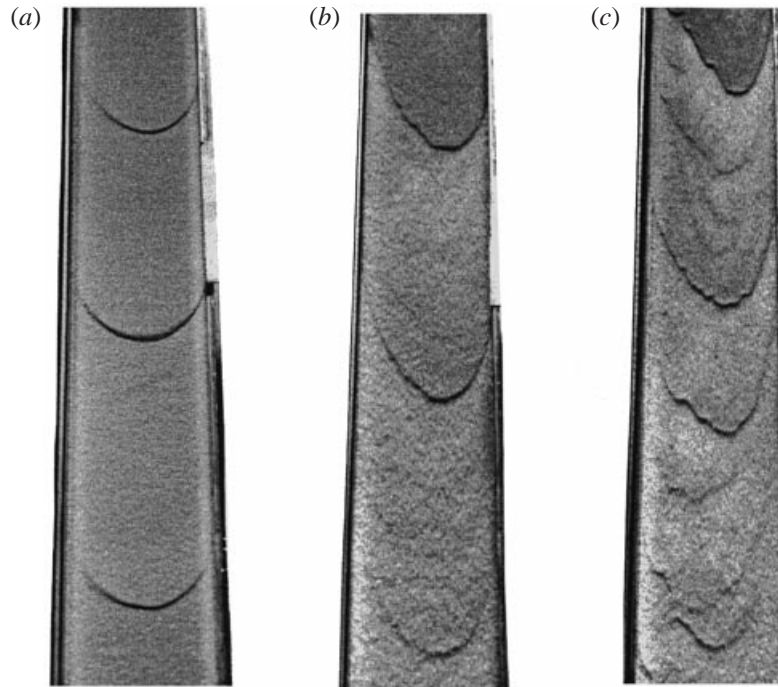
FIGURE 2. Representative flow visualization photographs of shallow granular flows at different flow conditions. The flow direction is from top to bottom. (a) $\theta = 30°, d_{av} = 106.5\,\mu m, Q = 1500\,g\,min^{-1}$, (b) $\theta = 35°, d_{av} = 213.5\,\mu m, Q = 2200\,g\,min^{-1}$, (c) $\theta = 38°, d_{av} = 151\,\mu m, Q = 1200\,g\,min^{-1}$.

approximately normal distributions. Visualization pictures of the two-phase flow are shown in figure 2 at different angular inclinations of the channel for various particle sizes. It can be observed that the wavelengths of the periodic structures did not remain absolutely constant at any x-location on the channel. This may be due to higher-order effects such as convective instabilities which force smaller waves to become consumed by larger waves. The wavefronts remained approximately axisymmetric, though larger nonlinearities were evident at higher wave velocities (e.g. in figure 2c). Other nonlinear effects such as evolution of the lateral structures (i.e. along the z-axis) near the wavefronts seem to be controlled by the depth-averaged longitudinal velocity (u) of the particles and the mean particle size (d_{av}). The origin of these structures lies in the rotational motion of particles about the y-axis which arises due to oblique impacts between the particles and the sidewalls. As long as a substantial fraction of the total kinetic energy of the particles is not represented by this rotational mode, the evolution of such lateral instabilities can be avoided. The shear at the sidewalls of the channel increased with the wave velocities and with increasing channel slope. It controlled the shape of the wavefronts along the z-axis and resulted in stretching of the waves. The effects of particle segregation normal to the inclined bed could not be observed since the flow depth was small. Some segregation of particles along the mean flow direction was observable at smaller flow rates and for particle mixtures of larger mean size. This effect can be enhanced further if coarser mixtures of particles, which contain a wider range of particle sizes, are tested at intermediate feed rates.

Figure 3 shows the measured average wavelengths at a distance of 2.5 m from the feeding point for three different angular inclinations of the channel. For $\theta = 30°$,
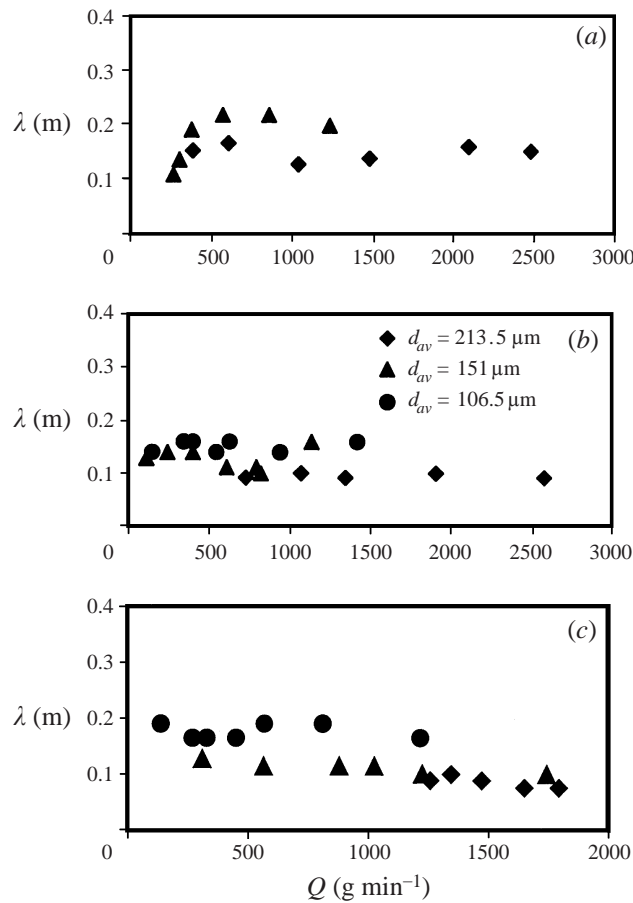
FIGURE 3. Variations of measured wavelength with material flow rate.
(*a*) $\theta = 30°$, (*b*) $\theta = 35°$, (*c*) $\theta = 38°$.

only two of the three size ranges of the spherical particles were used because the measurement uncertainty for the smallest size (i.e. $d_{av} = 106.5\,\mu m$) was quite high at that angular inclination. The corresponding wave velocities at these flow rates in figure 4 show that increasing the angular inclination of the channel resulted in an overall increase of wave velocities for all the three sizes of particles. For the purpose of accurate measurements of wavelengths and wave velocities, larger particles had to be tested at higher flow rates than those for the smaller particles. The selection of the range of flow rates (Q) for different particle sizes ensured that the wave features were pronounced for all the flow conditions. Though the measured wave velocities showed an increasing trend with increasing particle size, the average wavelength of the periodic structures did not show large variations for the three sizes of particles (figure 3). In fact, the average wavelength of the structures remained almost constant for the entire range of flow rates for any one size of the particles. It can, however, be noticed that for different sizes of particles tested at the same channel slope, smaller particles yielded comparatively larger wavelengths for similar material flow rates and vice versa. A possible explanation of this behaviour is presented in §6 after comparing the observed trend with theoretical predictions of a nonlinear wave model. In our experiments, no apparent longitudinal organization was visible for material
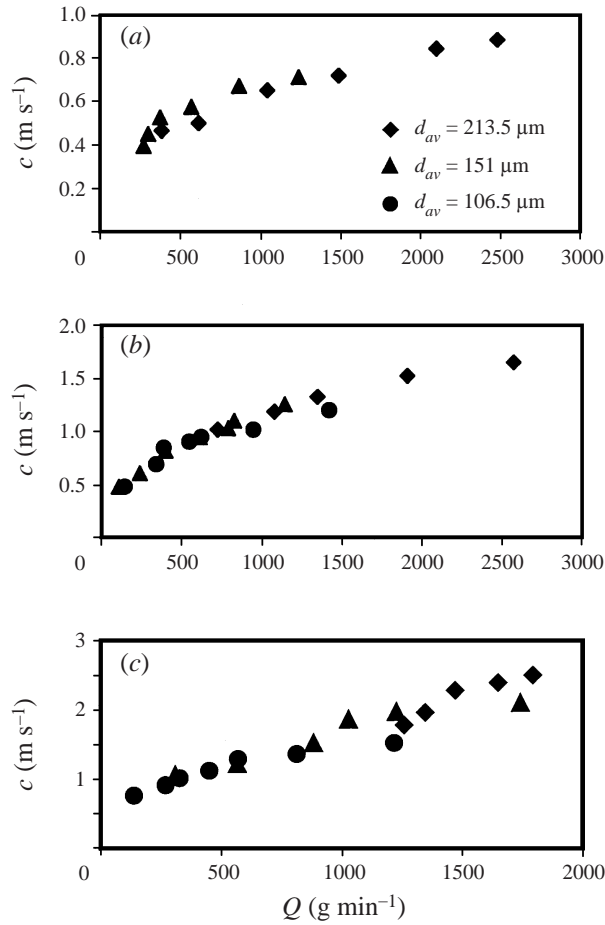
FIGURE 4. Variations of measured wave velocity with material flow rate.
(*a*) $\theta = 30°$, (*b*) $\theta = 35°$, (*c*) $\theta = 38°$.

flow rates less than $100 \, \text{g min}^{-1}$. The particles had very large saltating motions when the volumetric solid fractions were very low at such small flow rates. For flow rates higher than $2800 \, \text{g min}^{-1}$, the shockfronts became diffused and their motion could not be tracked with sufficient accuracy with the present video-taping technique. Though the grains still remain relatively dispersed at high flow rates, the collisional energy transfer between particles increased rapidly over most of the wavelength. It should, however, be mentioned that the flow regimes for longitudinal organization seem to be bounded by limits of both low and high flow rates for a particular channel surface condition and the present ranges of channel slope and particle size.

4. Revisiting granular transport processes

In this section, we review some of the relevant findings of previous research on granular flows with the intention of elucidating the context of the present theoretical model. It also helps in identifying a suitable approach to describe several aspects of the present organizational behaviour in flowing grains. In their investigation of the unsteady transport of a shallow layer of fluid mud, Ng & Mei (1994) and Liu & Mei (1994) have applied the shallow water theory in explaining the behaviour of

two-phase power-law fluids. Their theoretical approach suggested a gradual variation in the dissipational characteristics of the medium as roll waves evolve in the mixture flow. This variation in flow resistance is expected to be strongly dependent on the volumetric concentration of the solid phase and its local gradient. The existence of the periodic waves was found from an energy criterion which satisfied positive energy loss across the shockfronts. Following Dressler's (1949) analysis of discontinuous periodic flows in shallow water, Needham & Merkin (1984) included a diffusive term in the longitudinal momentum conservation equation to construct continuous periodic solutions to shallow fluid flows on an inclined surface. Such a diffusive term contributes significantly in the energy dissipation process only where there is a large longitudinal gradient of the mean flow velocity, i.e. $\partial u/\partial x$, near the discontinuity. Though this approach mathematically satisfies the periodicity conditions of the shallow fluid flow, it does not necessarily provide a universal definition of the dissipative agent which can be applied to shallow gravitational flows of grains. In fact, dispersed grain flows, which show a similar periodic nature of transport, have negligible longitudinal gradients of mean particle velocities in most of the flow field. The solid–gas mixture, rather, shows a marked variation in the volumetric density of the solid phase only near the wavefronts. As a result, the change in elevation of the free surface in shallow grain flows is much smaller than an analogous change in shallow water flow. Observation of the evolving structures in such grain flows shows them to possess periodicity with multiple wavelengths, though the length scales remain of the same order of magnitude. It appears that waves of greater height continue to grow at the expense of weaker waves and the resulting wavelengths elongate as they convect downstream in the channel.

At this point, it is essential to note the basic differences in rheological behaviour between shallow granular flows and their dense flow counterpart. The transport of dense granular solids in liquid and gaseous media has been investigated in the past via shear-flow experiments (Bagnold 1956; Savage 1979; Patton, Brennen & Sabersky 1987) and theoretical continuum models (Cowin 1974; Savage 1979, 1984; Haff 1983). The flow depths in these cases were very large (e.g. $h/d_{av} > 20$) compared to the shallow regime of granular flows reported in the present study. In such dense flows, the aggregates of solid particles are observed to move as a bulk material and particle layers tend to slide on one another as a response to the shear force. The inter-particle distance remains of the same order of magnitude as the average particle diameter. The particle collisions play a dominant role in the process of momentum transfer in this 'grain-inertia' regime of granular flow. As granular temperature is generated, the solid–fluid mixture experiences dilatation in both the normal and the longitudinal flow directions. In the experimental studies of Savage (1979) and Ahn, Brennen & Sabersky (1991), this dilatation in the two-phase mixture was exhibited in the density and velocity profiles across the depth of the flow. For loosely packed particles, the primary mechanism of generating the granular temperature is through a 'streaming process' where the transport of the randomly fluctuating energy is dominant only in the direction of mean motion. Consequently, this latter mode of energy generation becomes an anisotropic process. This variation in the rheological behaviour of granular flows has been appropriately described in Ahn & Brennen (1992), where a distinction in momentum transfer modes is made on the basis of relative magnitude of generation, conduction and dissipation of fluctuation energy in the gas–particle mixture.

On the basis of flow depth and the critical Froude number (Campbell, Brennen & Sabersky 1985), the chute flows of granular material have been categorized into two major classes: subcritical and supercritical. The Froude number, defined as the ratio

of inertial forces and gravitational forces, is expressed as $Fr = u/(gh)^{1/2}$, where g is the acceleration due to gravity. It has been observed in experimental studies (Brennen, Sieck & Paslaski 1983; Campbell *et al.* 1985) that rapidly moving supercritical flows in the entrance region of a channel often go through a transitional stage called the 'hydraulic jump' to attain a slowly moving subcritical state. The transition occurs through a shock that travels upstream and gradually makes the entire flow subcritical. Though such hydraulic jumps in dense granular packings tend to suggest an energy-restoring behaviour similar to fluid systems, they do not exhibit any periodic or quasi-periodic mode of transport as observed in shallow and dispersed grain flows. This difference only points to the fact that energy-cyclic processes and the evolving length and time scales in such granular flows have a strong dependence on the shallow free-surface condition of the flowing medium. It appears that in this cyclic process, the presence of an 'energy-escape window' is critical. The particle accumulation and the resulting collisional energy loss at the wavefront satisfy this condition.

5. Physical flow mechanism

In this section, a physical explanation of the observed transport process is presented. Since the two-dimensional shallow grain waves appear to be controlled by an energy-cyclic process, we here investigate a one-dimensional wave model which admits discontinuous periodic solutions and satisfies the energy-inequality condition across the discontinuities. It should be mentioned that in spite of our choice of a one-dimensional flow model for the sake of simplicity, it adequately establishes a flow criterion that explains the existence of longitudinal waves in an essentially two-dimensional flow field. Although the details of particle motions play an important role in the transport process, a continuum analysis in which average values of the dynamical parameters are used seems appropriate for understanding the large-scale wave phenomenon. As the solid particles roll down the inclined channel, the evolving periodic structure of the two-phase flow can be expressed in a continuum sense as shown in figure 5(*a*). The imaginary free-surface profile, as defined by the curved line on top, has been exaggerated to emphasize the variations in both the flow depth and the volumetric density of the solid phase near the wavefronts. The solid particles are dispersed in the interstitial fluid (i.e. fully submerged in air) and they are free to move relative to each other. The relative movement of the particles is assumed to be parallel to each other in the direction of mean flow (i.e. *x*-axis). The normal and lateral components of the particle velocity are assumed to be small compared to the longitudinal component of velocity. Dressler (1949) explained the evolution mechanism of nonlinear waves in shallow channel flows where the flow depth is small. He used the shock-fitted periodic solutions in a water flow situation where the density of the medium did not vary. In his treatment, the height of the free surface from the channel bed varied significantly within one wavelength of the roll waves. The same theoretical treatment is followed here with certain modifications for the solid–gas mixture.

We here assume that the particle layers are moving on top of each other in such a way that the resultant motion is primarily in the *x*-direction. Following the arguments of Patton *et al.* (1987), the total number of particle layers can be approximated as $N = (hv/d_{av})$, where v is the volumetric solid fraction of the material defined as the fraction of solid volume in the entire volume of the material. The resultant mixture density is defined as $\rho = v\rho_p$, where ρ_p is the material density of the solid spheres. The partial density of the gaseous phase has been neglected, because the ratio of
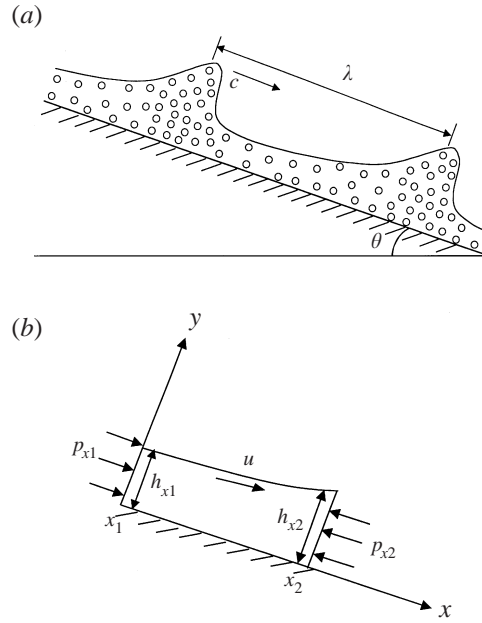
(a)

(b)

FIGURE 5. Schematic of periodic waves in shallow and dispersed granular flows. (a) Idealized flow field, and (b) control volume of dispersed flow region between wavefronts.

solid density to fluid density is very large. In the experiments described in §2, it was observed that the local particle velocity varied substantially as the acceleration and deceleration processes took place within the wavelength of individual flow structures. Therefore, the longitudinal component of the flow velocity (u) is a function of the longitudinal coordinate (x) and time (t) only. It is also assumed that the normal gradient of the longitudinal velocity is negligible, because the depth of flow is small compared to the average particle diameter. The mass and x-momentum conservation equations for the control volume of figure 5(b) can be expressed as

$$\frac{\partial N}{\partial t} + \frac{\partial}{\partial x}(Nu) = 0 \tag{1}$$

and

$$\frac{\partial u}{\partial t} + u\frac{\partial u}{\partial x} = -\tfrac{1}{2}g\cos\theta\left(\frac{\partial h}{\partial x} + \frac{h}{N}\frac{\partial N}{\partial x}\right) + g\sin\theta - \frac{T}{\rho_p N d_{av}}. \tag{2}$$

The first and second terms on the left-hand side of the depth-averaged x-momentum equation (2) represent the rate of change of momentum inside the control volume and the net transport of linear momentum across the control surface. The three terms on the right-hand side of (2) are the pressure force, the body force and the dissipative force, respectively. In the momentum equation, T denotes the total resistive stress on the moving particles per unit length of the control volume. The total resistance is provided by several physically distinct sources whose relative magnitudes vary with changes in the local volumetric solid fraction. However, in the theoretical development of shallow water waves, the resistance effects are considered in the lowest approximations of the fluid flow equations. This renders continuous wave profiles into asymmetric profiles with steepening of the free surface which ultimately leads to wave breaking (or shock).

The counterpart of dynamic shock in our shallow grain-flow experiments is the phenomenon of sudden build-up of the volumetric solid fraction at the wavefronts. Therefore, analogous resistance terms which preserve these flow features are examined here. For reasons discussed previously and examined later in this section, the resistive stress on the control volume can be replaced by the relationship $T = \alpha u^2$, since most of the resistance on the spherical particles is generated by viscous drag forces. Here, α denotes the dimensional proportionality constant and has dimensions of mass density. The relationship between the local stress and the average flow velocity is most accurate for the dispersed regions of particle motion where the inter-particle distances are large compared to the average particle diameter. It provides a micromechanical definition of energy dissipation in the rarefield flow regions. This assumption is equivalent to the condition that the shear stress at the channel bed is proportional to the square of the mean flow velocity. Such a boundary condition is allowable within the framework of a perturbation method which permits inclusion of resistive terms based on various flow-induced dissipative mechanisms.

In Ng & Mei (1994), the resistive shear stress in a shallow layer of a homogeneous power-law fluid has been assumed to be nonlinearly proportional to the normal gradient of the depth-averaged longitudinal velocity. Such a macroscopic definition of energy dissipation in a two-phase mixture also satisfied the instability conditions of evolving roll waves within a range of the proportionality coefficient. In shallow granular flows, the particle concentrations become large near the wavefronts. The actual drag coefficient on the assemblage of particles in these concentrated regions can be significantly different (Happel & Brenner 1965) than those in the rarefied regions where interactions between particles is almost insignificant. In the present physical model of shallow dispersed flows, the modifications to the actual drag coefficient due to the presence of the stationary solid boundary and due to higher-order interactions between adjacent particles have been neglected.

The pressure force term in (2) has two parts: one due to a change in flow depth and the other due to a change in the number of flowing particle layers. The change in N can occur by virtue of a change in the local value of v without altering the flow depth. This mechanism should depend on the momentum transfer modes (i.e. translational, rotational or vibratory) between layers of moving particles. It should be noted that though all the three flow variables h, N and v are dependent on one another, the present theoretical model only treats h and N as independent variables whereas v is considered a flow parameter. In the shallow and dispersed flow regions, the longitudinal variation of the volumetric solid fraction (i.e. $\partial v / \partial x$) is expected to be small and, therefore, the present parametric solution of the conservation equations should approximately represent the dynamics of the shallow granular flow. The quantity within parentheses on the right-hand side of (2) needs further examination for the present problem. The free-surface-induced part (i.e. $\partial h / \partial x$) is relatively very small over most of the domain where waves evolve, whereas the continuum effect by means of particulate hydrodynamic interactions occurs through the longitudinal gradient of the particle layer number (i.e. $\partial N / \partial x$). It is in this respect that our hydrodynamic model of shallow granular flow differs from the classical roll wave analysis. With the aforesaid assumptions, the modified x-momentum equation for shallow flows is written as

$$u_t + u u_x = -K_1 N_x + K_2 - K_3 \frac{u^2}{N}, \tag{3}$$

where $K_1 = (g d_{av} \cos \theta / v), K_2 = g \sin \theta$ and $K_3 = (\alpha / \rho_p d_{av})$ are system coefficients.

The subscripts x and t denote differentiation with respect to the longitudinal flow direction and time, respectively. With this combination of the flow parameters, the x-momentum equation (3) has now been reduced to the same form as in shallow water theory (Dressler 1949). We, therefore, adapt the analysis of shallow fluid flows on inclined planes, though the inclusion of v in coefficient K_1 and the velocity dependence of α in coefficient K_3 make the internal mechanisms of wave propagation distinct from that of roll waves in water.

In order to examine the behaviour of longitudinal waves in a two-phase flow, the flow variables in the moving coordinate system are defined (i.e. with respect to the shock) as

$$\left.\begin{array}{l} u(x,t) = U(x - ct) = U(\xi), \\ N(x,t) = n(x - ct) = n(\xi), \\ u_x = U', \quad u_t = -cU', \quad N_x = n', \quad N_t = -cn', \end{array}\right\} \tag{4}$$

where c is the velocity of the moving shock in the positive x-direction. The prime denotes differentiation with respect to ξ, which is the coordinate with respect to the moving observer at the shock. It is assumed that the velocity of the wavefront is not a function of x. In the case of particle flows where dispersive forces are dominant in the energy distribution process, the wave velocity can be expected to depend on x. For the present experiments, dispersion is introduced in the flow field via the non-uniformity of particle sizes. Therefore, its effect on the wave velocity is neglected in the proposed physical model of the flow. In the moving coordinate system, the mass and longitudinal momentum conservation are

$$nU' + (U - c)n' = 0 \tag{5}$$

and

$$(U - c)U' + K_1 n' = K_2 - K_3 \frac{U^2}{n}. \tag{6}$$

From the algebraic equations (5) and (6), the expressions for n' and U' can be solved. As a result, the wave profile equation and the velocity distribution are obtained as

$$n'(\xi) = \frac{K_3 U^2 - K_2 n}{(U - c)^2 - K_1 n} \tag{7}$$

and

$$U'(\xi) = \frac{(U - c)\left(K_2 - K_3 U^2/n\right)}{(U - c)^2 - K_1 n}. \tag{8}$$

Equation (7) shows the profile of the free surface in terms of the gradient of the total number of particle layers in the moving reference frame. Equation (8) shows the corresponding variation of the longitudinal component of average particle velocity. From (7) and (8), the apparent discharge rate of the two-phase medium is obtained. This apparent discharge rate (K) is the amount of the solid–gas mixture carried per unit time as observed from the moving reference at the wavefront. Dividing (7) with (8), we obtain

$$\frac{\mathrm{d}n}{\mathrm{d}U} = \frac{n}{c - U} \tag{9}$$

which when integrated yields the apparent discharge rate with respect to the moving shock front as

$$K = (c - U)n. \tag{10}$$

This discharge is the same at any point in the flow as long as the observation point is fixed on the wavefront. The profile equation (7) can now be expressed in terms of the apparent discharge rate as

$$n' = -\frac{n[K_2 - K_3(cn - K)^2/n^3]}{K^2/n^2 - K_1 n}. \tag{11}$$

Equation (11) is the profile equation of the free surface. Dressler (1949), in his analysis of shallow water waves, showed that both the numerator and the denominator of (11) should be zero at the critical flow point (i.e. at the point where $U = (gh)^{1/2}$) for a realistic solution for the wave profile. He referred to this criterion as the 'special' solution for the existence of the nonlinear water waves. This special solution provides a sufficient condition for satisfying the energy inequality across the discontinuities of the surface profile. The same arguments hold well in the case of shallow granular flows where the steepening of the wavefronts corresponds to an increase in the number of particle layers (N). Furthermore, it should be noted that the dissipation of fluctuation energy at the wavefronts automatically satisfies this energy loss criterion. The location of the critical flow in the moving coordinate system is a finite distance away from the shock. Therefore, the free surface remains closely parallel to the *x*-axis instead of showing a discontinuity at that point. The flow depth increases rapidly only near the vicinity of the shock. Following Dressler's shock-fitting analysis, the special solution at the critical point of the flow is obtained. The critical flow parameters, in terms of the wave velocity and the system constants, are

$$U_0 = \frac{c}{1 + (K_3 K_1/K_2)^{1/2}}, \quad n_0 = \frac{c^2 K_3/K_2}{[1 + (K_3 K_1/K_2)^{1/2}]^2}, \quad K_0 = K_1^{1/2} n_0^{3/2}, \tag{12}$$

where the subscript zero denotes a variable evaluated at the critical point. Since the apparent discharge rate is the same at all points in the flow relative to the moving shock, it can be replaced in (11) by the expression in (12). Therefore, the profile equation (11) can now be written in terms of the critical number of particle layers, n_0, as

$$n' = \frac{s[n^3 + pn^2 + qn + r]}{(n - n_0)[n^2 + nn_0 + n_0^2]}, \tag{13}$$

where the coefficients of the third-order polynomial in n in the numerator are given by

$$p = -\left(\frac{K_3 c^2}{K_2}\right), \quad q = 2cK_1^{1/2} n_0^{3/2} \frac{K_3}{K_2}, \quad r = \frac{-K_3 K_1}{K_2} n_0^3, \quad s = \frac{K_2}{K_1}.$$

The numerator of (13) can be factorized so that the critical solution (i.e. $n = n_0$) is eliminated. So, the final form of the profile equation becomes

$$n' = \frac{s[n^2 + (n_0 - K_3 c^2/K_2)n + (K_3 K_1/K_2)n_0^2]}{n^2 + nn_0 + n_0^2}. \tag{14}$$

The numerator of (14) has to be positive so that the slope of the free surface remains positive at all points except for the point of discontinuity. This necessary condition yields the physical criterion for which the progressive waves would exist in shallow two-phase flows. The necessary physical criterion is obtained by substituting for the system constants K_1, K_2, K_3 and n_0 in the numerator of (14). Thus, we get

$$m > 4\epsilon \tag{15}$$

where $m = \tan\theta$ and $\epsilon = (\alpha/v\rho_p)$. This is exactly similar to the criterion for the existence of nonlinear roll waves in shallow water flows down an inclined surface. For the short-wavelength approximation, the limiting expression for the wave velocity becomes

$$\lambda \to 0: \quad c \to \left[\frac{gZ}{1/[1 + \sqrt{m/\epsilon}]^2 - 1/[1 + \sqrt{m/\epsilon}]^3}\right]^{1/3}, \quad (16)$$

where Z is the average volumetric discharge rate per unit span of the control volume (see Dressler 1949). The corresponding wave velocity for the long-wavelength approximation is

$$\lambda \to \infty: \quad c \to$$
$$\left[\frac{gZ}{(\sqrt{\epsilon}/2m)(\sqrt{\epsilon} + 2\sqrt{m} + [(\sqrt{\epsilon} + 2\sqrt{m})^2 - 4m]^{1/2})/[1 + \sqrt{m/\epsilon}]^2 - 1/[1 + \sqrt{m/\epsilon}]^3}\right]^{1/3}.$$
$$(17)$$

In both (16) and (17), the wave velocity increases as the cube root of the average discharge rate. Since the actual wave velocity is expected to lie between these limits, both approximations are investigated in the present computations. Our experimental observations suggest that the average volumetric discharge rate becomes a function of the wavelength (λ) of the periodic flow structures. The average of this volumetric flow rate, Z, is obtained by integrating the instantaneous discharge rate at a fixed point over an entire wavelength of flow. The instantaneous flow rate through a fixed point on the chute (i.e. stationery observer) is time varying and is repeated over each local time period of the waves.

In the above analysis, the system constants, K_1 and K_2, are known for a given mixture of solid and gas, average diameter of the solid spheres, average volumetric solid fraction of the solid–gas mixture, and angular inclination of the channel. Since the variation in the volumetric solid fraction could not be measured accurately within one wavelength of the flow, solutions given in equation (16) and (17) are represented parametrically within a feasible range of average v values. The third system constant, K_3, involves the proportionality constant α (and therefore ϵ) which is not known *a priori*. Since the present analysis explores the possible similarity of the grain waves to shallow water waves, it is expected that K_3 would play a similar role as that of the resistance coefficient in the roll-wave theory. As mentioned earlier, the particle motion in the dispersed flow regions is primarily in the rolling mode with intermittent bed contact; the particles remain airborne for a considerable period of time during their passage down the channel. In this mode of transport, the total energy loss due to sliding contact with the bed is expected to be insignificant. This is also evident from the study of Jan & Chen (1997) in which the coefficient of sliding friction for isolated particle motion on a smooth surface was estimated to be of the order of 10^{-2}. If U_0 represents the average longitudinal component of particle velocity, then the corresponding particle Reynolds number is

$$Re_p = \left(\frac{\rho_f U_0 d_{av}}{\mu}\right). \quad (18)$$

The velocity of the critical flow point is a satisfactory representation of the average velocity because the profile of the free surface still remains parallel to the channel bed. In our computations, the critical velocity has been calculated from (12). For this

purpose, a curve-fitted variation of the measured wave velocity at the observation point has been used as a first approximation for obtaining the critical velocity. The range of computed Reynolds numbers for the present experimental conditions was $3 < Re_p < 35$. The drag coefficient for isolated spheres in the Reynolds number range $0 < Re_p < 2 \times 10^5$ is given by (White 1991)

$$C_D \approx \frac{24}{Re_p} + \frac{6}{1 + \sqrt{Re_p}} + 0.4. \tag{19}$$

In the rarefied flow region, each particle has been assumed to be fully submerged in air. The pressure drop across the freely moving spheres can, therefore, be neglected. The average resistance coefficient, ϵ_{av}, is expressed in terms of the average drag coefficient (C_D) as

$$\epsilon_{av} = \frac{\rho_f C_D}{2 v \rho_p}. \tag{20}$$

Since the determination of U_0 depends on ϵ_{av} and vice versa, (18) and (20) are iteratively solved to reach convergence for the average resistance coefficient. The underlying reason for adopting the iterative technique is that the nonlinear wave model employed here is not fully determinate. The model predicts continuous dependence of wavelength on wave velocity within the window of opportunity of wave existence. The iterative procedure adopted here overcomes the difficulty due to this indeterminacy and clearly leads to a converging solution. The maximum volumetric solid fraction, v_∞, for spherical particles can be as high as 0.74 for a fully packed bed of spherical grains. Patton *et al.* (1987) experimentally obtained a value of $(v/v_\infty) = 0.6$ for deep chute flows where N becomes larger than 4. In the present theoretical computations, the numerical value of the average volumetric solid fraction is varied within a physically acceptable range ($v = 0.1$ to 0.5) for comparatively rarefied flows to investigate its effect on the wave velocity.

6. Theoretical predictions

This section reports the theoretically predicted wave velocities for varied conditions of shallow grain flow. In our analysis, the variables U_0, c and ϵ_{av} yield certain continuous surfaces in the phase space, showing their interdependence through (12), (20), (16) and (17). As mentioned in the previous section, the estimation of ϵ_{av} in (20) depends on the estimation of U_0. In the present computations, the value of U_0 in (12) is dependent on c. Our experiments, however, show that only a limited range of wavelengths and wave velocities are physically possible. This means that the length and time scales are chosen through a physically realizable selection process, e.g. minimization of certain energies. Therefore, in order to solve the interdependence of (12), (20), (16) and (17) in our analysis, an initial estimate of U_0 was obtained using the experimental data on the wave velocity. Least-square fits were obtained on the experimental values of c for this purpose. Within the experimental range of θ and d_{av}, the approximate functional relationship between the wave velocity and the mass-flow rate was $c = aQ^b$, where a and b are constants given in table 1. This value of c was used in (12) to obtain a first approximations for U_0 for any value of Q. Once the initial estimate of U_0 was available in this way, (18) and (20) were iteratively solved for convergence of ϵ_{av}. During this iteration, the functional form of c in (12) is kept unaltered from its initial approximate form. Such an approximation for the initial estimate of U_0 is appropriate in the present context since the variation

θ (deg.)	d_{av} (μm)	a	b
30	151	0.056	0.364
	213.5	0.051	0.365
35	106.5	0.069	0.400
	151	0.066	0.417
	213.5	0.075	0.396
38	106.5	0.147	0.333
	151	0.082	0.439
	213.5	0.002	0.943

TABLE 1. Values of the nonlinear curve-fitting coefficients relating the observed wave velocity relation (i.e. $c = aQ^b$) for a range of channel slope and average particle size.

in particle velocities with varying material feed rate is expected to be very similar to the variation of wave velocities.

For the small wavelength approximation (16), the predictions show closer agreement with the measured wave velocities. The long-wavelength approximation (17) tends to overestimate the wave velocities for all experimental conditions, though the predictions still remain of the same order of magnitude as that of the measured wave velocities. As the mean size of the particles is increased, while keeping the channel inclination unaltered, the predicted values of wave velocity also increase. This is expected since greater mass of an individual particle induces larger magnitude of particle momentum in the flow. Therefore, the overall flow momentum is also enhanced. Figure 6 shows the computed wave velocities from (16) and their comparison to the measured wave velocities at three different inclinations (θ) of the channel. The assumed value of the average volumetric solid fraction is 0.1 in these predictions. For the present set of experimental parameters, the theoretically predicted wave velocities are slightly higher at the minimum θ (i.e. 30°) and slightly lower at the maximum θ (i.e. 38°). This trend seems consistent with the experimental observations. At lower channel inclinations, the extent of energy loss in sliding friction and inter-particle collisions can be expected to be larger than that at higher channel inclinations. The mean particle velocities are reduced at smaller channel slopes and the absence of substantial fluidization (i.e. large-amplitude saltating motions) increases the contact time of individual particles with the channel surface and with other particles. This results in enhanced energy dissipation over that caused by interstitial fluid drag only. Therefore, the present theoretical predictions of wave velocity, which account for energy dissipation through viscous drag, are higher than the measured wave velocities at $\theta = 30°$. As the channel inclination increases, the energy loss through sliding friction and inter-particle collisions in dispersed flow regions becomes less significant. The predicted wave velocities at $\theta = 38°$ are lower than the measured wave velocities because the assumed value of the volumetric solid fraction (i.e. $v = 0.1$) is probably an overestimation in this case. Higher channel slopes aid in causing enhanced fluidization of the granular medium and, as a result, the mean volumetric solid fraction reduces further. The effect of diminishing solid fraction on the wave velocity is discussed later in this section. It is evident that in the absence of accurate estimates of v in the rarefied flow regions, the theoretical predictions only reveal the trend in variations of wave velocities with changing material feed rate. The short-wavelength limit of
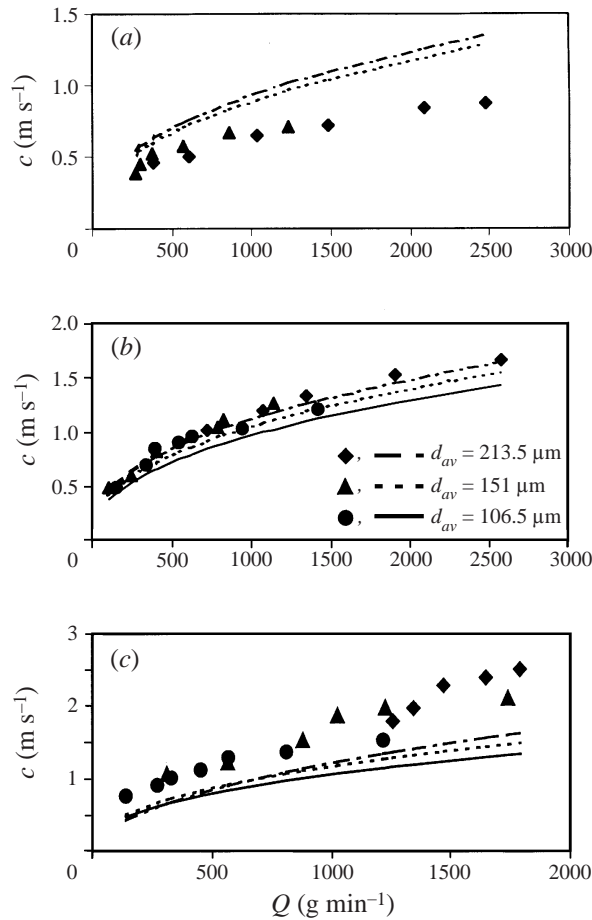
FIGURE 6. Comparison of measured and predicted wave velocities.
(*a*) $\theta = 30°$, (*b*) $\theta = 35°$, (*c*) $\theta = 38°$.

approximation shows that a reduction in the volumetric solid fraction of the mixture in the range $0.1 < v < 0.5$ results in higher particle velocities and, therefore, higher wave velocities. In contrast, the long-wavelength limit suggests a stronger but opposite dependence on the assumed value of the solid fraction. In that case, the predicted wave velocities are reduced to the order of measured wave velocities if the magnitude of v is made very small (e.g. ~ 0.02). Both the short- and long-wavelength limits of approximation show implicit dependence on the magnitude of ϵ_{av} which varies inversely with v. Therefore, the prediction behaviour of (16) and (17) with varying v still remains purely parametric unless a true representation of the average solid fraction is available for all experimental conditions.

The computations also revealed the magnitude of the average resistance coefficient for different flow conditions. In the present study, m has been varied in the range of 0.57 to 0.78. The estimated magnitudes of ϵ_{av} in the theoretical computations varies between 0.001 and 0.03. The corresponding range of values for K_3 was between 2.13 and 26.36. The inequality in (15) has, therefore, been satisfied for all the flow situations studied here. It can be noticed that the values of the non-dimensional resistance coefficient (ϵ_{av}) are at least an order of magnitude smaller than the sliding

+ $v = 0.5, d_{av} = 106.5$ μm   ◆ $v = 0.5, d_{av} = 151$ μm   ■ $v = 0.5, d_{av} = 213.5$ μm

✕ $v = 0.3, d_{av} = 106.5$ μm   ▲ $v = 0.3, d_{av} = 151$ μm   ○ $v = 0.3, d_{av} = 213.5$ μm

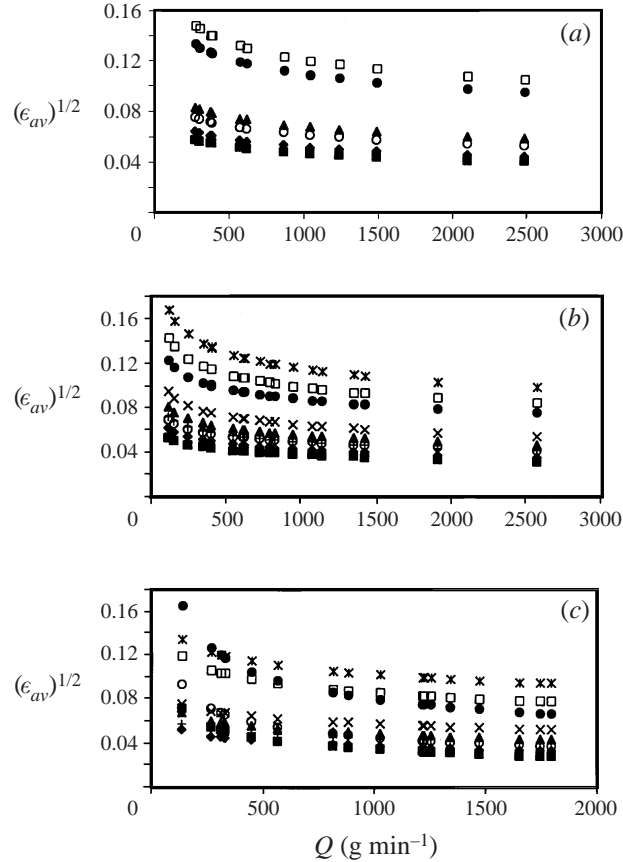✱ $v = 0.1, d_{av} = 106.5$ μm   □ $v = 0.1, d_{av} = 151$ μm   ● $v = 0.1, d_{av} = 213.5$ μm

FIGURE 7. Variation of the average viscous resistance with volumetric solid fraction and material flow rate. (*a*) $\theta = 30°$, (*b*) $\theta = 35°$, (*c*) $\theta = 38°$.

Coulombic frictional coefficient between glass spheres and an aluminium channel. The variations of $(\epsilon_{av})^{1/2}$ with Q, v and θ are shown in figure 7. As v decreases, the average resistance coefficient increases nonlinearly. Therefore, it is to be expected that the wave velocities would also increase nonlinearly at sufficiently small values of the volumetric solid fraction. Though the average viscous resistance seems to decrease asymptotically with increasing Q, the wave velocities increase almost monotonically with increasing Q. The estimation for Z in equations (16) and (17) was made from Q and an average value of the volumetric solid fraction (e.g. $v = 0.1$ in figure 6). Figure 8 shows the difference in the magnitude of predicted wave velocities from equation (16) for different values of v, θ, and d_{av}. As v is changed in the same order of magnitude (which seems to be physically possible in this kind of shallow flow), it does not change the predicted value of c to a large extent.

The measurements of wavelengths in figure 3 show some remarkable features which confirm our adoption of viscous drag as the primary flow resistance mechanism. For particles tested at the same channel slope, it can be noticed that the observed
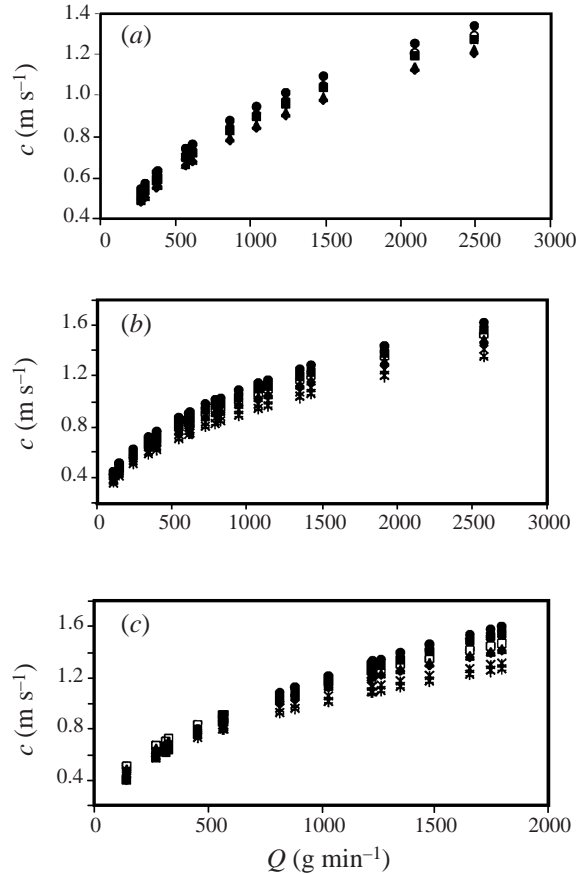
FIGURE 8. Variation of the predicted wave velocity with volumetric solid fraction and material flow rate. (a) $\theta = 30°$, (b) $\theta = 35°$, (c) $\theta = 38°$.

wavelength increases when the average diameter of the particles is reduced. This is due to the fact that smaller particles have larger specific surface area ($A_s \propto d_{av}^{-1}$) which increases the specific resistance in the dispersed flow field. As the specific resistance increases, it takes the particle mass longer to produce sufficient magnitude of the fluctuation energy to be suddenly dissipated to form the shockfront. This results in lengthening of average wavelengths on the channel bed. The selection of average wavelength also depends on the rate of availability of the potential energy given by the channel slope and the specific shock energy which depends on the average particle size. As the channel slope increases, the average wavelength is observed to decrease which indicates an enhanced rate of generation of fluctuation energy in the granular flow. Similar trends are also observed in the roll-wave analysis of Dressler (1949). His numerical results on the variations of specific shock energy as a function of wavelength clearly show that the preferred wavelength decreases when the magnitude of the specific shock energy increases. Also, the probability of attaining definite shockfronts of substantial shock energy is enhanced for flows having smaller

values of the average resistance coefficient. Smaller magnitude of energy dissipation in the rest of the wavelength ensures the availability of enough fluctuation energy to be dissipated at the shockfront. Our experimental observations of the progressive longitudinal waves in shallow granular flows corroborate these predictions of the dynamic flow model.

7. Concluding remarks and discussions

In shallow and dispersed granular flows on inclined channels, the threshold condition for generating longitudinal grain waves is achieved beyond a minimum critical flow rate when the large-scale saltating motions normal to the channel bed are diminished in magnitude. A practically homogeneous and dispersed mixture of moving solid particles in still gas exists in a fluidized state and the initiation of longitudinal waves seems probable. The viscous drag force on the moving particles represents the most pertinent dissipating agent in such a fluidized state. Resistance to flow due to sliding friction between particles and the boundaries should, therefore, be negligible. Once fluidization is attained, combinations of certain ranges of channel slope, mean grain size and material flow rate exhibit longitudinal waves in the flow field. Increasing flow rate results in an energy-cyclic process, where excess kinetic energy is allowed to escape through the formation of shocks in the concentration domains. Also, at higher flow rates, variations in the periodic free-surface profile are enhanced through an increase in the effective depth of flow. Beyond an upper bound of grain flow rates, significant particulate interactions occur throughout the flow field causing isotropic conduction of fluctuation energy through dilatational effects. Consequently, the granular organizations become diffused.

Our experiments revealed the existence of longitudinal wave features in the overall transport process of grains. These longitudinal wave modes seem to constitute the primary organizations through which the momentum redistributions establish an energy cycle in the flow. This is especially true for rapidly moving shallow granular flows which exhibit large particle velocities in most of the longitudinal flow structures. This rapid flow condition can be termed a fully inertial regime of shallow granular flows. Under certain flow conditions, however, lateral wave modes appear due to nonlinear dispersion and sheared flow near the sidewalls. Though the existence of kinematic waves in one-dimensional two-phase flows (Wallis 1969) has also been investigated in the past, the present phenomenon of progressive waves appears to be primarily dynamic in nature, i.e. the balance between the flow inertia and dissipative stresses determines the nature of the evolving waves. The kinematic wave theory of Lighthill & Whitham (1955) seems to relate more to the non-energetic (i.e. slowly moving) unsteady flow conditions at even lower channel inclinations. In that case, particulate organization can occur in a semi-inertial regime of grain flows where wave velocities are generally less than the particle velocities.

In the present chute-flow experiments, all solid particles go through a process of acceleration and deceleration as the moving wavefront passes through the two-phase medium. A particulate hydrodynamic model similar to Dressler's (1949) roll-wave model is examined here to provide an insight into the dynamic processes. The periodic nature of this kind of grain flow is similar to that of shallow liquid flows. The only major difference between the two cases is that the variation in the resultant material density becomes an additional important parameter in solid–gas mixture flows. The formulation through the particle layer number N, however, provides a means by which Dressler's (1949) nonlinear wave analysis could be utilized. The

essence of this discontinuous periodic solution lies in the possibility of an energy inequality across the wavefronts. Energy loss through particulate interactions in the wavefronts encountered in our experiments satisfies this inequality condition. The present theoretical analysis of the shallow grain flow remains parameteric in the absence of pertinent information like the longitudinal variations of the particle velocity and the volumertric solid fraction in the dispersed flow regions. However, the modified one-dimensional wave model does seem to correlate the large-scale dynamic flow parameters with our experimental data. It shows the physical criterion for which these longitudinal waves would evolve and sustain themselves in dispersed two-phase flows. It also presents the qualitative trends in the wave mode of transport in layered particulate flows.

REFERENCES

AHN, H. & BRENNEN, C. E. 1992 Channel flows of granular materials and their rheological implications. In *Particulate Two-Phase Flow* (ed. M. Roco). Butterworth-Heinemann.

AHN, H., BRENNEN, C. E. & SABERSKY, R. H. 1991 Measurements of velocity, velocity fluctuations, density and stresses in chute flows of granular materials. *J. Appl. Mech.* **58**, 792–803.

BAGNOLD, R. A. 1956 The flow of cohesionless grains in fluids. *Phil. Trans. R. Soc. Lond.* A **249**, 235–297.

BRENNEN, C. E., SIECK, K. & PASLASKI, J. 1983 Hydraulic jumps in granular material flow. *Powder Tech.* **35**, 31–37.

CAMPBELL, C. S., BRENNEN, C. E. & SABERSKY, R. H. 1985 Flow regimes in inclined open channels. *Powder Tech.* **41**, 77–82.

COWIN, S. C. 1974 A theory for the flow of granular materials. *Powder Tech.* **9**, 61–69.

DRESSLER, R. F. 1949 Mathematical solution of the problem of roll waves in inclined open channels. *Commun. Pure Appl. Maths* **2,** 149–194.

FRIED, E., SHEN, A. Q. & THORODDSEN, S. T. 1998 Wave patterns in a thin layer of sand within a rotating horizontal cylinder. *Phys. Fluids* **10**, 10–12.

HAFF, P. K. 1983 Grain flow as a fluid mechanical phenomenon. *J. Fluid Mech.* **134**, 401–430.

HAPPEL, J. & BRENNER, H. 1965 *Low Reynolds Number Hydrodynamics*. Prentice-Hall.

IVERSON, R. M. 1997 The physics of debris flow. *Rev. Geophys.* **35**, 245–296.

JAN, C.-D. & CHEN, J.-C. 1997 Movements of a sphere rolling down an inclined plane. *J. Hydraul. Res.* **35**, 689–706.

JOHNSON, P. C., NOTT, P. & JACKSON, R. 1990 Frictional-collisional equations of motion for particulate flows and their application to chutes. *J. Fluid Mech* **210**, 501–535.

LIGHTHILL, M. J. & WHITHAM, G. B. 1955 On kinematic waves. I. Flood movement in long rivers. *Proc. R. Soc. Lond.* A **229**, 281–316.

LIU, K.-F. & MEI, C. C. 1994 Roll waves on a layer of muddy fluid flowing down a gentle slope – A Bingham model. *Phys. Fluids* **6**, 2577–2590.

NEEDHAM, D. J. & MERKIN J. H. 1984 On roll waves down an open inclined channel. *Proc. R. Soc. Lond.* A **394**, 259–278.

NG, C.-O. & MEI, C. C. 1994 Roll waves on a shallow layer of mud modelled as a power-law fluid. *J. Fluid Mech.* **263**, 151–183.

PATTON, J. S., BRENNEN, C. E. & SABERSKY, R. H. 1987 Shear flows of rapidly flowing granular materials. *J. Appl. Mech.* **54**, 801–805.

POULIQUEN, O., DELOUR, J. & SAVAGE, S. B. 1997 Fingering in granular flows. *Nature* **386**, 816–817.

SAVAGE, S. B. 1979 Gravity flow of cohesionless granular materials in chutes and channels. *J. Fluid Mech.* **92**, 53–96.

SAVAGE, S. B. 1984 The mechanics of rapid granular flows. *Adv. Appl. Mech.* **24**, 289–366.

WALLIS, G. B. 1969 *One-Dimensional Two-Phase Flow*. McGraw-Hill.

WHITE, F. M. 1991 *Viscous Fluid Flow*. McGraw-Hill.